Earth and Planetary Science Letters 319-320 (2012) 23–34

Contents lists available at SciVerse ScienceDirect

Earth and Planetary Science Letters

journal homepage: www.elsevier.com/locate/epsl

Mantle structure beneath Africa and Arabia from adaptively parameterized P-wave tomography: Implications for the origin of Cenozoic Afro-Arabian tectonism

Samantha E. Hansen [a,*], Andrew A. Nyblade [b], Margaret H. Benoit [c]

[a] Geological Sciences Department, University of Alabama, Tuscaloosa, AL 35487, USA
[b] Geosciences Department, Pennsylvania State University, University Park, PA 16802, USA
[c] Physics Department, The College of New Jersey, Ewing, NJ 08628, USA

ARTICLE INFO

Article history:
Received 1 November 2011
Received in revised form 19 December 2011
Accepted 21 December 2011
Available online 20 January 2012

Editor: P. Shearer

Keywords:
tomography
Africa
Arabia
superplume
rifting

ABSTRACT

While the Cenozoic Afro-Arabian Rift System (AARS) has been the focus of numerous studies, it has long been questioned if low-velocity anomalies in the upper mantle beneath eastern Africa and western Arabia are connected, forming one large anomaly, and if any parts of the anomalous upper mantle structure extend into the lower mantle. To address these questions, we have developed a new image of P-wave velocity variations in the Afro-Arabian mantle using an adaptively parameterized tomography approach and an expanded dataset containing travel-times from earthquakes recorded on many new temporary and permanent seismic networks. Our model shows a laterally continuous, low-velocity region in the upper mantle beneath all of eastern Africa and western Arabia, extending to depths of ~500–700 km, as well as a lower mantle anomaly beneath southern Africa that rises from the core-mantle boundary to at least ~1100 km depth and possibly connects to the upper mantle anomaly across the transition zone. Geodynamic models which invoke one or more discrete plumes to explain the origin of the AARS are difficult to reconcile with the lateral and depth extent of the upper mantle low-velocity region, as are non-plume models invoking small-scale convection passively induced by lithospheric extension or by edge-flow around thick cratonic lithosphere. Instead, the low-velocity anomaly beneath the AARS can be explained by the African superplume model, where the anomalous upper mantle structure is a continuation of a large, thermo-chemical upwelling in the lower mantle beneath southern Africa. These findings provide further support for a geodynamic connection between processes in Earth's lower mantle and continental break-up within the AARS.

1. Introduction

The Cenozoic Afro-Arabian rift system (AARS), characterized by crustal extension, volcanism, and plateau uplift across much of eastern Africa and western Arabia (Fig. 1), is arguably one of the best places to investigate geodynamic processes leading to continental break-up. Many body wave tomography models have shown that the Arabian Shield, as well as the East African and Ethiopian Plateaus, are underlain by upper mantle low-velocity anomalies that could be connected beneath the southern Red Sea and the Turkana Depression (Fig. 1) to form one, large upper mantle structure. Parts of this structure could also extend through the transition zone into the lower mantle (*e.g.* Bastow et al., 2008; Benoit et al., 2003, 2006a; Nyblade et al., 2000; Park et al., 2007, 2008; Ritsema et al., 1999). However, because these models are based on seismic networks with limited aperture, it is difficult to determine whether or not the anomalies are actually parts of the same upper mantle structure or to ascertain their depth extent. Tomography models using surface waves also show slow upper mantle velocities in this region (Debayle et al., 2001; Fishwick, 2010; Pasyanos and Nyblade, 2007; Priestley et al., 2008; Sebai et al., 2006; Sicilia et al., 2008), but the lateral resolution associated with such models is generally several hundred kilometers, which is too large to resolve separate upper mantle anomalies beneath different parts of the AARS. The corresponding vertical resolution of these models is also limited below ~300–400 km depth, making it difficult to determine if the anomalies extend through the transition zone.

The lateral and depth extent of the upper mantle low-velocity anomalies beneath East Africa, Ethiopia, and western Arabia has important implications for understanding the origin of tectonism within the AARS. Three types of geodynamic models have been proposed to explain the rifting, volcanism, and plateau uplift found in this region. The first type of model invokes small-scale convection, either resulting from lithospheric stretching (Fig. 2a; Buck, 1986; Mutter et al., 1988) or from edge-flow from beneath the Congo craton (Fig. 2b; King, 2007; King and Ritsema, 2000). The second group of models includes one or more mantle plumes beneath eastern Africa and western Arabia (Fig. 2c; *e.g.* Camp and Roobol, 1992; Chang and van der

* Corresponding author.
E-mail address: shansen@geo.ua.edu (S.E. Hansen).

0012-821X/$ – see front matter © 2011 Elsevier B.V. All rights reserved.
doi:10.1016/j.epsl.2011.12.023

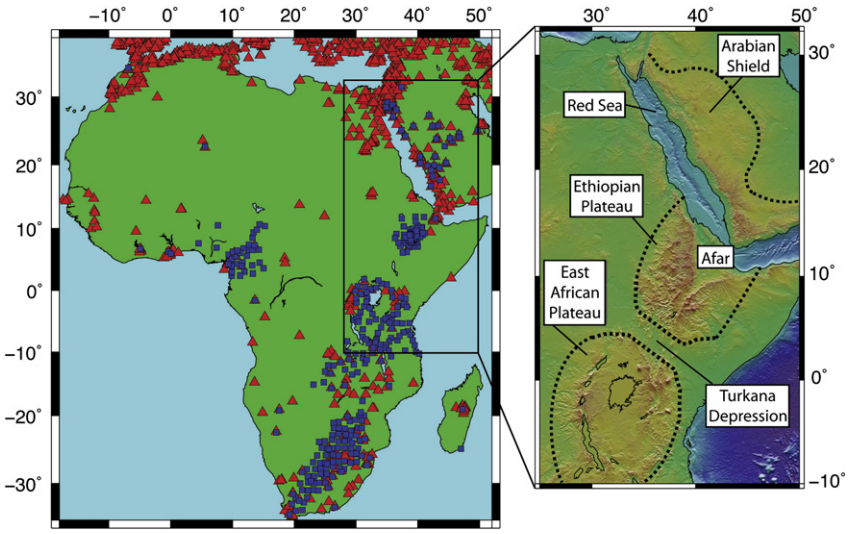

Fig. 1. Maps of study area and station distribution. (left) Distribution of stations used in our tomographic inversion. Red triangles denote stations included in the EHB database while blue squares denote stations from the augmented dataset. (right) Close-up of the Afro-Arabian region with topography from the 30 s digital elevation map in GMT (Wessel and Smith, 1998). Dashed lines show the extent of the East African and Ethiopian Plateaus as well as the Arabian Shield. Important topographic features are labeled.

Lee, 2011; Ebinger and Sleep, 1998; George et al., 1998; Montelli et al., 2006), and these models are characterized by ~100–200 km thick plume head material ponded beneath the lithosphere, fed by a narrow (~100–200 km diameter) plume tail. The final category of models attributes the origin of the AARS to a feature commonly referred to as the African superplume (Fig. 2d; *e.g.* Bastow et al., 2008; Benoit et al., 2006b; Forte et al., 2010; Furman et al., 2006; Park and Nyblade, 2006; Ritsema et al., 1999; Simmons et al., 2007, 2009), which is thought to be a large, thermo-chemical anomaly that develops near the core-mantle boundary beneath southern Africa and that tilts northeastward beneath eastern Africa at mid-mantle depths. Because the different types of geodynamic models would result in different upper mantle anomalies, the nature of the upper mantle structure across the AARS can be used to evaluate them.

To further investigate the lateral and depth extent of the upper mantle anomalies beneath the AARS, we have developed a new tomographic image of P-wave speed variations in the African and Arabian mantle using an adaptive parameterization method (Kárason, 2002; Li et al., 2008). An expanded dataset containing travel-times from earthquakes recorded on many new permanent and temporary seismic networks throughout the study region has also been employed. This approach leads to a P-wave tomography model with improved resolution of mantle structure beneath the AARS compared to many previous models, thereby enabling us to reevaluate geodynamic models for the origin of the Cenozoic tectonism in this area.

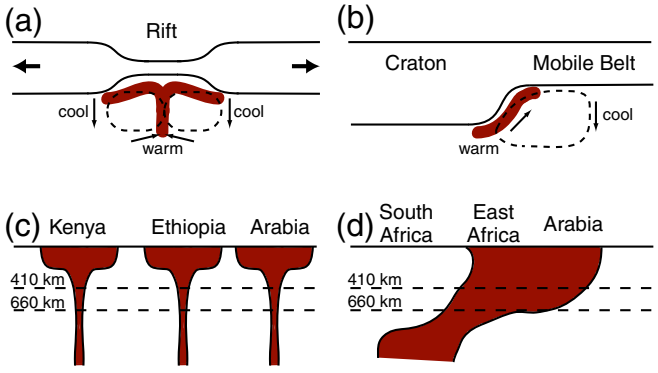

Fig. 2. Origin models for the AARS. Cartoons illustrating different geodynamic origin models that have been proposed for the AARS, including (a) small-scale convection induced by lithospheric stretching, (b) small-scale convection resulting from edge-flow, (c) plume models, and (d) the superplume model.

2. Background and previous studies

2.1. Global seismic models

Using global tomographic models, a number of authors over the past decade have commented on mantle structure beneath Africa and Arabia. Based on a 3-D shear-wave model, the study by Ritsema et al. (1999) was one of the earliest to suggest that the African superplume structure might be linked to Cenozoic tectonism in eastern Africa and Arabia. Mégnin and Romanowicz (2000) made a similar suggestion based on their model of shear-velocity heterogeneity, and a possible connection between anomalous lower and upper mantle structure beneath Africa was apparent in several other shear wave models that were published at about the same time (*e.g.* Grand, 2002; Gu et al., 2001; Masters et al., 2000). More recently, Simmons et al. (2007, 2009, 2010) developed global models using both shear-wave travel times and geodynamic observations, and in these models, the African superplume is interpreted as a low-density, thermo-chemical structure extending upwards from the core-mantle boundary to depths of at least ~1500 km. Eastern Africa is also underlain by an upper mantle low-density structure, but the authors stated that it is unclear whether this feature is connected to the deeper mantle. A recent model by Ritsema et al. (2011) highlights anomalously slow shear velocities extending through the lower mantle beneath southern Africa, but this study also mentions that the connection between the superplume and the upper mantle beneath eastern Africa might be less certain than suggested by Ritsema et al. (1999).

Using a global P-wave tomographic model, Montelli et al. (2006) examined the depth extent of various mantle plumes. Similar to Simmons et al. (2007, 2009, 2010), they imaged the superplume extending upwards from the core-mantle boundary to a depth of ~1500 km. The Montelli et al. (2006) model also shows low-velocity anomalies in the upper mantle beneath Afar and East Africa, and the authors suggest that these anomalies originate at mid-mantle depths or deeper. Using the same methodology as the current study, Li et al. (2008) developed a global model of P-wave velocity perturbations. While not discussed in detail, their model shows low velocities throughout much of the upper mantle beneath eastern Africa and

western Arabia as well as the lower mantle superplume anomaly. The recent study by Simmons et al. (2011) used a global P-wave model to examine upper mantle structures in the Middle East, somewhat outside of our study area, but their model illustrates that slow seismic velocities down to at least 300 km depth underlie Ethiopia and western Arabia and may be continuous beneath the southern Red Sea.

2.2. Continental and regional seismic models

Continental- and regional-scale body wave studies have also provided many details about the mantle structure beneath Africa and Arabia. Using both P- and S-wave travel-times, Ritsema et al. (1998a) imaged ~200 km thick lithosphere beneath the Tanzania craton in the center of the East African Plateau and a low-velocity region to the east of the craton, extending to depths below 400 km. Nyblade et al. (2000) used receiver functions to illustrate that the transition zone beneath Tanzania is thinned by 30–40 km and suggested that a mantle plume may underlie this area. Benoit et al. (2006a, 2006b) imaged P- and S-wave velocity perturbations beneath Ethiopia and identified a wide (>500 km) low-velocity region also extending to depths >400 km. Bastow et al. (2005, 2008) made similar observations and suggested that the low P- and S-wave velocities reflect the upper mantle continuation of the African superplume. Park and Nyblade (2006) examined the P-wave structure beneath Kenya and imaged a westward dipping low-velocity structure extending to depths >300 km, consistent with a connection to the lower mantle superplume anomaly. In contrast, Chang and Van der Lee (2011) examined the structure beneath eastern Africa and Arabia using a joint inversion of regional and teleseismic S phases, as well as other constraints, and they found elongated low-velocity anomalies extending to ~1400 km depth, which they interpreted as separate mantle upwellings beneath Kenya and Afar.

Surface wave tomography has also provided significant insight to the mantle structure beneath Africa. In the continental-scale models of Sebai et al. (2006), Pasyanos and Nyblade (2007), and Priestley et al. (2008), low shear-wave speeds are seen beneath eastern Africa, the Red Sea, and the Gulf of Aden, extending to depths of at least 350 km. These models also illustrate that high velocity roots are present beneath cratonic regions, down to ~200–250 km. Fishwick (2010), whose model is focused on central and southern Africa, showed similar results. On a more regional scale, Debayle et al. (2001) imaged a low-velocity anomaly that persists down to 660 km depth beneath Afar and suggested that their observations are best explained by either a cluster of several narrow plume tails or by a region of broad mantle upwelling. These findings are consistent with those of Sicilia et al. (2008), who modeled S_v velocities and anisotropy beneath Afar and concluded that the hotspot must have a deep origin. Weeraratne et al. (2003) suggested that low velocities imaged beneath the Tanzania craton are consistent with a plume centered beneath the East African Plateau and that thermal perturbations may be present down to depths ≥660 km.

In Arabia, Benoit et al. (2003) imaged a low P-wave velocity anomaly in the upper mantle, extending from the Red Sea eastward into the interior of the Arabian Shield, but associated receiver function analysis did not show thinning of the transition zone beneath this region, suggesting that the low velocities are concentrated above 410 km. A similar study by Park et al. (2007) showed low P- and S-wave velocities along the western side of the Arabian Shield, and the authors favored either a single plume or a superplume model to explain their observations. Surface wave tomography models have also shown a broad low-velocity region across the Arabian Shield, extending to depths ≥150 km along the Red Sea coast, and Park et al. (2008) suggested that this anomalous structure results from flow beneath the southern Red Sea, with a connection to the anomaly beneath Ethiopia. Chang et al. (2011) jointly inverted body and surface wave data and imaged slow seismic velocities beneath the southern Red Sea. They have suggested that mantle flow is not directed beneath the axis of the Red Sea but rather northward from Afar beneath the Arabian Peninsula.

2.3. Additional studies

Other approaches have also provided insights into the mantle structure and geodynamics beneath Africa and Arabia. Some mantle convection models, which were developed from tomographic images of wave-speed variations, indicate that dynamic topography supported by the African superplume can explain both the high surface elevations observed across southern and eastern Africa (Forte et al., 2010; Gurnis et al., 2000; Lithgow-Bertelloni and Silver, 1999; Moucha and Forte, 2011) as well as the tilt of the Arabian plate (Daradich et al., 2003), suggesting that the upper mantle anomalies beneath East Africa, Ethiopia, and western Arabia are all part of the same geodynamic system. However, other numerical models do not agree with this assessment. Lin et al. (2005) advocated for two distinct mantle plumes beneath eastern Africa, while Ebinger and Sleep (1998) suggested that one plume impinging beneath the Ethiopian Plateau, with flow channelized by lithospheric topography into the surrounding regions, could explain the distribution of uplift and volcanism in this region. Alternatively, Buck (1986) and Mutter et al. (1988) have suggested that no mantle upwellings are required and that rifting is the result of induced small-scale convection beneath lithosphere that has been stretched by extensional stresses along the edges of the African plate (Fig. 2a). Small-scale convection has also been suggested by King and Ritsema (2000) and King (2007), but in their models differences in heat flux between the thicker lithosphere beneath the Congo craton and thinner lithosphere beneath the surrounding mobile belts lead to rifting above a small-scale thermal upwelling (Fig. 2b).

Numerous geochemical studies of the AARS, many more than can be reviewed here, have also led to a variety of interpretations. For example, George et al. (1998) used $^{40}Ar/^{39}Ar$ age determinations to argue for two separate plumes beneath Ethiopia and Kenya, and Rogers et al. (2000) and Nelson et al. (2008) reached similar conclusions using Sr, Nd, and Pb isotope ratios. Pik et al. (2006), who examined helium isotopic measurements, suggested that two types of mantle plumes are present beneath Africa: a large, deep-seated plume that possibly originates near the core-mantle boundary and a second-order upwelling originating at a depth less than 400 km. On the other hand, Furman et al. (2006) and Furman (2007) argued that major and trace element compositions of basalts from eastern Africa support a common, large-scale upwelling originating at deep mantle depths (*i.e.* the African superplume). Camp and Roobol (1992) examined the compositions of lavas from various Cenozoic volcanic fields. Coupled with other observations, they concluded that the Arabian Shield is thermally supported by hot, upwelling asthenosphere from either a mantle plume centrally located beneath Arabia or from channelized flow originating beneath Ethiopia.

Ultimately, while the AARS has been the focus of many studies, considerable controversy about the nature of the upper mantle structure beneath eastern Africa and Arabia still remains. Whether the anomalous geochemical and geophysical characteristics of the upper mantle in this region result from a common origin has important implications for understanding what processes have led to rifting, volcanism, and plateau uplift within the AARS.

3. Data and methodology

As explained above, to further examine mantle structure beneath Africa and Arabia, we have developed a new P-wave tomographic image using the inversion method of Kárason (2002) and Li et al. (2008). This approach uses travel-time residuals from local, regional, and teleseismic phases calculated with respect to travel-times

predicted by the global ak135 Earth model (Kennett et al., 1995). The largest source of global travel-time residuals used is the reprocessed International Seismological Centre database from Engdahl et al. (1998; hereinafter referred to as the EHB database), which includes a wide range of seismic phases (*e.g.* P, Pg, Pn, pP, PKP) to maximize the effective sampling of the Earth's structure. The EHB catalog used in this study includes over 15 million travel-time residuals associated with more than 496,000 earthquakes, which occurred in the time period between January 1964 and October 2007.

Many of the African stations included in the EHB database only operated for short periods of time and their distribution is sparse compared to many other regions of the globe (Fig. 1). Additionally, much new data has become available since October 2007, when the EHB catalog ends. Therefore, we have augmented the EHB dataset with P-wave travel-times recorded by many new permanent seismic stations in Africa belonging to the AfricaArray network (www.africaarray.org), as well as by temporary seismic networks operated over the past two decades in Saudi Arabia, Cameroon, Nigeria, Uganda, Ethiopia, Tanzania, Zimbabwe, Botswana, and South Africa (Fig. 1; Supplemental Table 1).

The AfricaArray data, which comprise about 20% of the augmented dataset, have been manually picked, and the associated mean arrival time standard deviation is approximately 0.10 s. Arrival time picks from other networks were obtained from regional studies (Bastow et al., 2008; Benoit et al., 2003, 2006b; Mulibo et al., 2011; Park et al., 2007; Reusch, 2009), where relative arrival time residuals were determined with a multichannel cross-correlation technique (MCCC; VanDecar and Crosson, 1990). In order to account for the relative times produced by MCCC, origin time corrections have been applied to these data. The mean arrival time standard deviation associated with the cross-correlated picks is 0.02 s. Great care has been taken in combining these different datasets, and Supplemental Fig. 1 illustrates the consistency of our travel-time residuals both between the EHB catalog and the augmented data, as well as between the handpicked and cross-correlated travel-time measurements. In total, the augmented dataset includes over 37,000 travel-time residuals. To balance the smaller but high-quality augmented dataset against the larger but somewhat noisier EHB catalog, we give the augmented data extra weight in the inversion (Kárason and van der Hilst, 2001; Li et al., 2008).

The combined EHB and Africa–Arabia dataset has been inverted for a global model of mantle structure using an iterative least-squares approach (Nolet, 1985; Paige and Saunders, 1982). As described by Li et al. (2008), the misfit function ($\boldsymbol{\varepsilon}$) is minimized by:

$$\boldsymbol{\varepsilon} = ||\boldsymbol{Am}-\boldsymbol{d}||^2 + k_1||\boldsymbol{Lm}||^2 + k_2||\boldsymbol{m}||^2 + k_3||\boldsymbol{C}-\boldsymbol{M_c}||^2$$

where $\boldsymbol{A}$ is the sensitivity matrix, $\boldsymbol{m}$ is the vector of model parameters, $\boldsymbol{d}$ is the data vector of travel-time residuals, $\boldsymbol{L}$ is a smoothing operator, and k_i are regularization terms used to damp noisy data and to find the best model with variations that are small relative to the reference model. Experiments with different combinations of k_i weighting were performed to determine appropriate values, but the choice of these parameters is subjective. The small incidence angles of P-waves may cause crustal anomalies to 'smear' to deeper depths in the model; therefore, the final term on the right-hand side of the equation corrects for crustal structure through regularization, where $\boldsymbol{C}$ is an *a priori* 3-D crustal model (CRUST2.0; Bassin et al., 2000) and $\boldsymbol{M_c}$ is the crustal part of the model space. This approach balances the crust and upper mantle contributions to the misfit and recovers the *a priori* crustal model (Li et al., 2006, 2008). Global inversions are performed in order to account for mantle heterogeneities outside the study area.

Kárason (2002) and Li et al. (2008) provide a full description of the sensitivity matrix calculations. Briefly, for short-period data with a center frequency of ~1 Hz, the data are back-projected along raypaths calculated in the ak135 reference model. Weighted composite rays are used to reduce the size of the sensitivity matrix (Kárason and van der Hilst, 2001; Spakman and Nolet, 1988). For long-period data, 3-D sensitivity kernels are approximated following Kárason and van der Hilst (2001). This approach allows the low-frequency data to constrain long wavelength structure without preventing short-period data from resolving smaller scale structures.

Significant lateral variations in resolution may result from uneven seismic raypath coverage in the mantle, and most tomographic techniques use a regularly-spaced grid, which tends to either overemphasize poorly sampled regions or average out small-scale structures. To mitigate the effects of uneven data coverage, the tomographic method employed here constructs an adaptable grid based on the sampling density of the high-frequency data (Abers and Roecker, 1991; Bijwaard et al., 1998; Kárason and van der Hilst, 2000). The adaptive grid is developed by combining one or more cells from a base grid (~0.7° in latitude and longitude and 45 km in depth) until a minimum ray density (900 hit counts) in each cell is obtained (Kárason, 2002; Li et al., 2008). The total number of sampled, adaptive cells used in our inversion is ~530,000. Examples of the adaptive grid developed for our P-wave tomography model are illustrated in Supplemental Fig. 2. Regions with finer grid spacing indicate areas with increased ray coverage, where improved resolution can be obtained.

4. Results and resolution tests

P-wave velocity perturbations (δV_P) at selected mantle depths are shown in Fig. 3, with cross-sections provided in Fig. 4. These results were obtained after 200 iterations of the inversion and correspond to a 93% reduction of the error function. The relative length of the residual vector dropped from 0.95 to 0.30 s. At shallow depths ($\leq$400 km), low velocities are prevalent beneath all of eastern Africa and western Arabia, with a very pronounced anomaly situated beneath Ethiopia and Afar. Slow velocities are also seen beneath the Cameroon volcanic line, while fast velocities delineate cratonic regions in southern, central, and western Africa (Fig. 3). Across the study area, wave speed variations range from approximately $\pm$1.5–2%, similar to other P-wave models of Africa and Arabia (*e.g.* Bastow et al., 2005, 2008; Benoit et al., 2003, 2006b; Park and Nyblade, 2006; Park et al., 2007), but the Ethiopia-Afar anomaly is more pronounced, with δV_P ~3–4% slower than the reference model.

As shown in both map view and cross-section, the slow seismic velocities beneath the AARS continue down through the transition zone, extending to depths of ~700 km beneath East Africa and western Arabia and to ~900 km beneath Ethiopia (Figs. 3–4). The low wave-speeds in the upper mantle appear to be laterally continuous, from beneath Tanzania in the south to the eastern side of the Arabian Peninsula in the north. We also observe a large, low-velocity anomaly that extends from near the core-mantle boundary beneath southern Africa to the northeast at mid-mantle depths (Fig. 4), consistent with images of the superplume from previous studies (*e.g.* Li et al., 2008; Montelli et al., 2006; Ritsema et al., 1998b, 1999, 2011; Simmons et al., 2007, 2009, 2010).

To assess model resolution, several tests were performed. First, to examine lateral resolution, checkerboard tests were constructed with an input pattern of 5°-wide anomalies with alternating $\pm$2% velocity variations. Synthetic travel-times were created and inverted using the same model parameterization as was used for the data. Noise was added to the synthetic travel-times as a Gaussian residual time error with a standard deviation of 0.04 s. This is a weighted average of the arrival time standard deviation for our augmented data. The resolution of our model varies spatially given the uneven station distribution, but our checkerboard pattern is well-recovered at most upper mantle depths beneath southern and eastern Africa and Arabia and more broadly at mid-mantle depths (Fig. 5). Our best amplitude

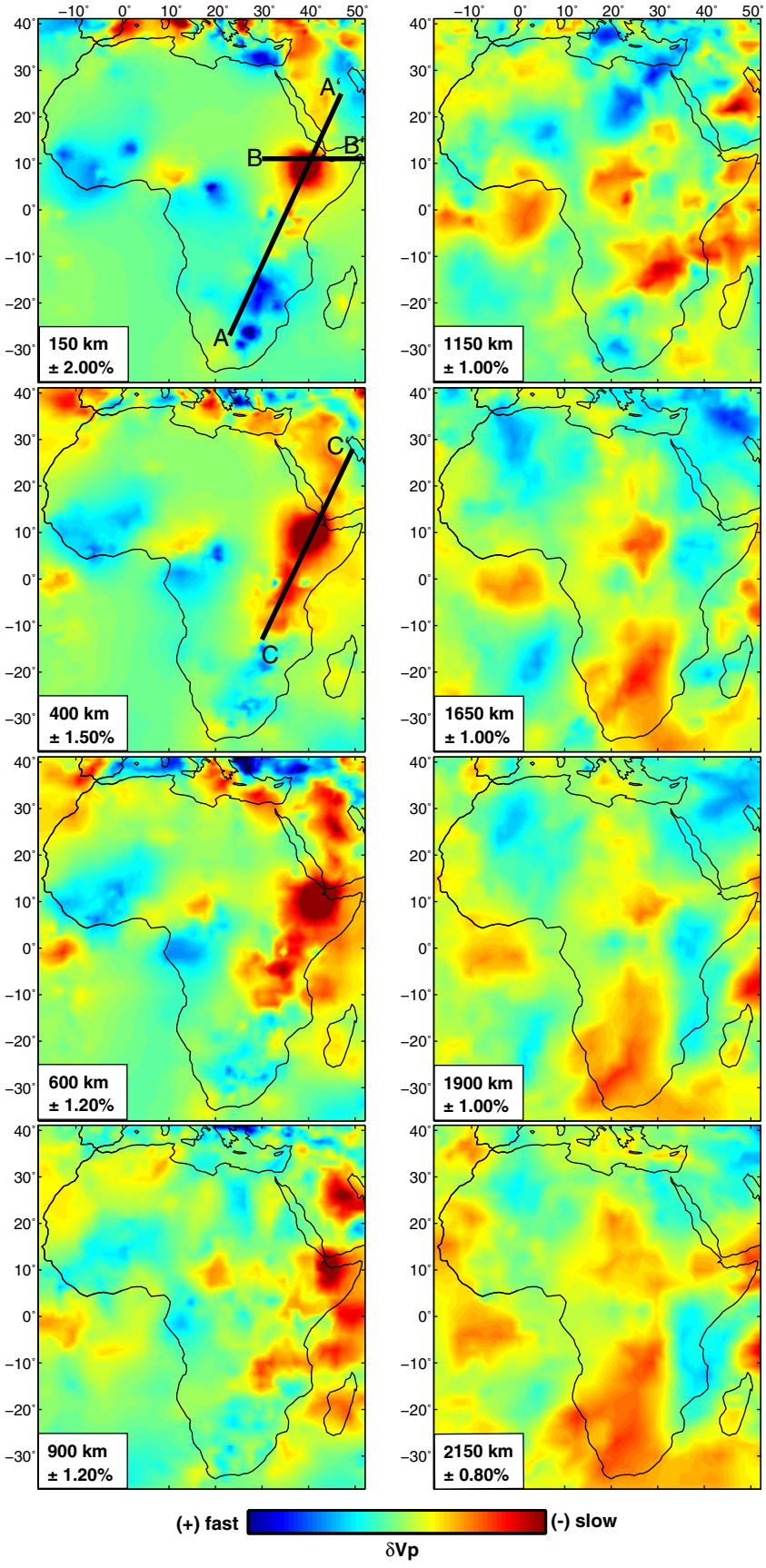

Fig. 3. New P-wave tomography image. P-wave velocity perturbations are shown at selected depths in the mantle. The ± values in each inset indicate the bounds of the color scale used for the corresponding panel. The locations of profiles A–A′ and B–B′ (Fig. 4) as well as C–C′ (Fig. 6) are shown in the 150 and 400 km depth panels.

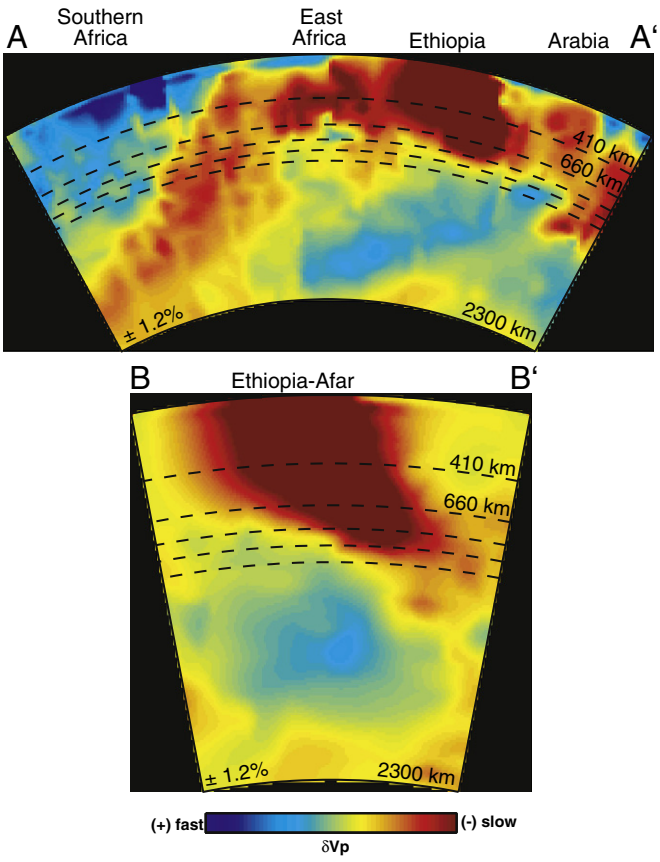

Fig. 4. Cross-sections through the tomographic image. Cross-sectional view of the P-wave tomography model along profiles A–A′ (top) and B–B′ (bottom), highlighting the low-velocity features in the African and Arabian mantle. Dashed lines mark the 410 and 660 km discontinuities as well as depths of 800, 900, and 1000 km.

recovery is ~50–70% due, in part, to regularization parameters used in the inversion to suppress the effects of noise in the data.

For comparison, checkerboard tests were also generated for a dataset equivalent to that used by Li et al. (2008; Supplemental Fig. 3). In the Li et al. (2008) study, which used the same methodology as employed here, travel-time residuals from 154 stations examined by Benoit et al. (2006b) were included as part of their supplemental dataset to the EHB catalog. This improved their resolution in southern and eastern Africa. These same data are also included in the current model, along with travel-time residuals from an additional 251 new stations. As shown in Fig. 5, our model has improved resolution, particularly at upper mantle depths beneath the study region.

Second, the extent of vertical smearing in our model was examined with synthetic anomalies in the upper and lower mantle (Fig. 6). Beneath eastern Africa and Arabia, the synthetic structure in the upper mantle is laterally continuous to match the anomaly in our model (Fig. 4), and the thickness of the anomaly was varied from 200 to 400 km. In the lower mantle, the synthetic structure is similar to the superplume beneath southern Africa. Since the checkerboard resolution tests indicate that the amplitude recovery of our model is ~50–70% (Fig. 5), we have roughly doubled the observed velocity perturbations, giving the upper and lower mantle synthetic anomalies input amplitudes that are 3% and 1.2% slower than the reference model, respectively. The recovered images show ~200 km of vertical smearing at all depths (Fig. 6), which is not atypical for P-wave tomography studies (*e.g.* Benoit et al., 2003, 2006b; Fouch et al., 2004; Park et al., 2007). It is interesting to note that if this level of vertical smearing is taken into account, the depth extent of the Kalahari, Congo, and West African cratons (Figs. 3–4) is ~200 km, which agrees well with estimates of cratonic lithospheric thickness from previous studies (Fishwick, 2010; Fouch et al., 2004; Pasyanos and Nyblade, 2007; Priestley et al., 2008; Romanowicz, 2009; Sebai et al., 2006).

The vertical resolution of the velocity anomalies observed in our model was also assessed with a series of squeeze tests (Allen and Tromp, 2005; Saltzer and Humphreys, 1997; Schutt and Humphreys, 2004). Squeezing was implemented through a two-stage inversion. During the first stage, damping parameters were specified such that the velocity anomalies were only permitted within a particular depth-range of the model. The residual data vector (*i.e.* the travel-time data that cannot be satisfied by velocity anomalies within the permitted depth-range) were then input into the second stage of the inversion, where the anomalies are allowed throughout the model. If the residuals from the first stage of inversion are zero, no new structure will be generated once the "squeezing" is removed in the second stage (Allen and Tromp, 2005; Saltzer and Humphreys, 1997; Schutt and Humphreys, 2004). However, if a better model exists, significant structure outside the initial constrained domain will develop once the velocity anomalies are allowed throughout the model space. Synthetic examples are provided in Supplemental Fig. 4.

To test the vertical extent of the upper mantle low-velocity anomaly in our tomographic model, squeezing depths ranging from 200 to 800 km were used to constrain the velocity perturbations to shallower portions of the model space (Fig. 7; Supplemental Fig. 5a). The extent of the lower mantle anomaly was also tested, but in this case the squeezing depths, which range between 600 and 2100 km, constrain the perturbations to progressively deeper portions of the model space (Supplemental Fig. 5b). The depth constraints provided by the squeezing approach are similar to those indicated by our resolution tests. For instance, the low velocity anomaly beneath Ethiopia appears to extend to ~900 km depth in our model (Fig. 4), but the squeeze tests indicate this feature can likely be constrained to depths ≤~700 km (*i.e.* ~200 km shallower; Fig. 7). However, the slow velocities throughout the transition zone are a prevalent feature, as is the lower mantle superplume anomaly, which extends up toward the transition zone and possibly crosses the 660 km discontinuity (Supplemental Fig. 5).

5. Discussion

The primary features of interest in our tomographic model are the upper mantle, low-velocity anomaly beneath eastern Africa and western Arabia and the lower mantle superplume anomaly. The upper mantle structure is laterally continuous from the southern end of the East African Plateau northeastward to the eastern side of the Arabian Peninsula, and given the results of our resolution tests, extends to depths of ~500–700 km throughout this region (Fig. 4). The superplume structure in our model possibly connects to the anomalous upper mantle structure across the transition zone just to the southwest of the East African Plateau. As mentioned previously, three types of geodynamic models have been proposed to explain the origin of rifting, volcanism, and plateau uplift in the AARS. In the following sections, the nature of the mantle beneath Africa and Arabia highlighted by our results is examined in relation to these models to gain new insights into the causes of Cenozoic tectonism.

5.1. Plume models

The first group of models attributes the origin of the AARS to mantle plumes, invoking plume head material ~100–200 km thick ponded beneath the lithosphere and fed by a narrow (~100–200 km diameter) plume tail (Fig. 2c; Davaille et al., 2005; Ebinger and Sleep, 1998; Montelli et al., 2006). However, amongst these models, there is little consensus about the number of plumes beneath eastern Africa and western Arabia. Ebinger and Sleep (1998),

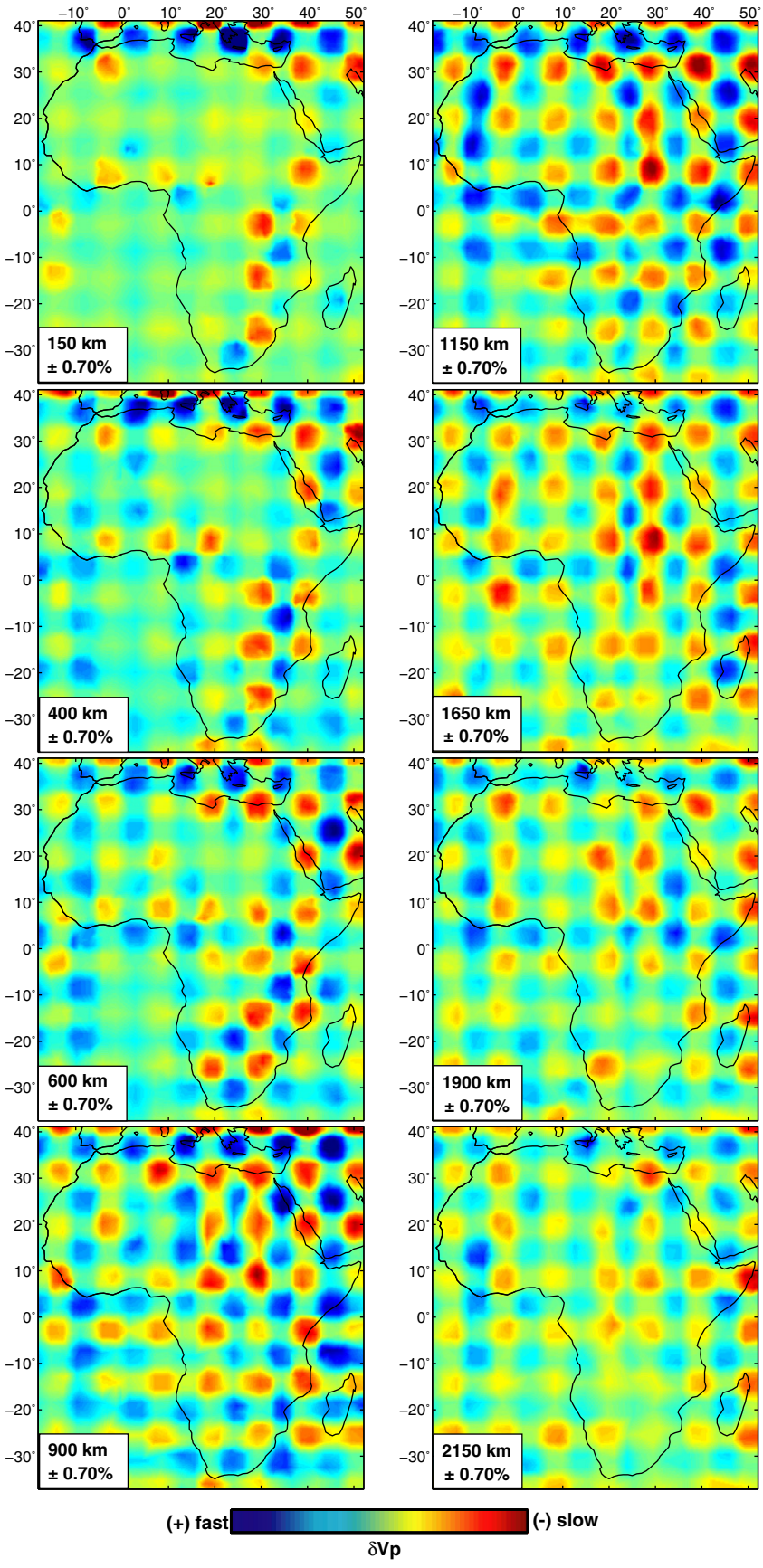

Fig. 5. Checkerboard resolution tests. Results from the checkerboard resolution tests, shown at selected mantle depths. All images have been plotted with the same color scale so that the degree of pattern and amplitude recovery can be easily compared.

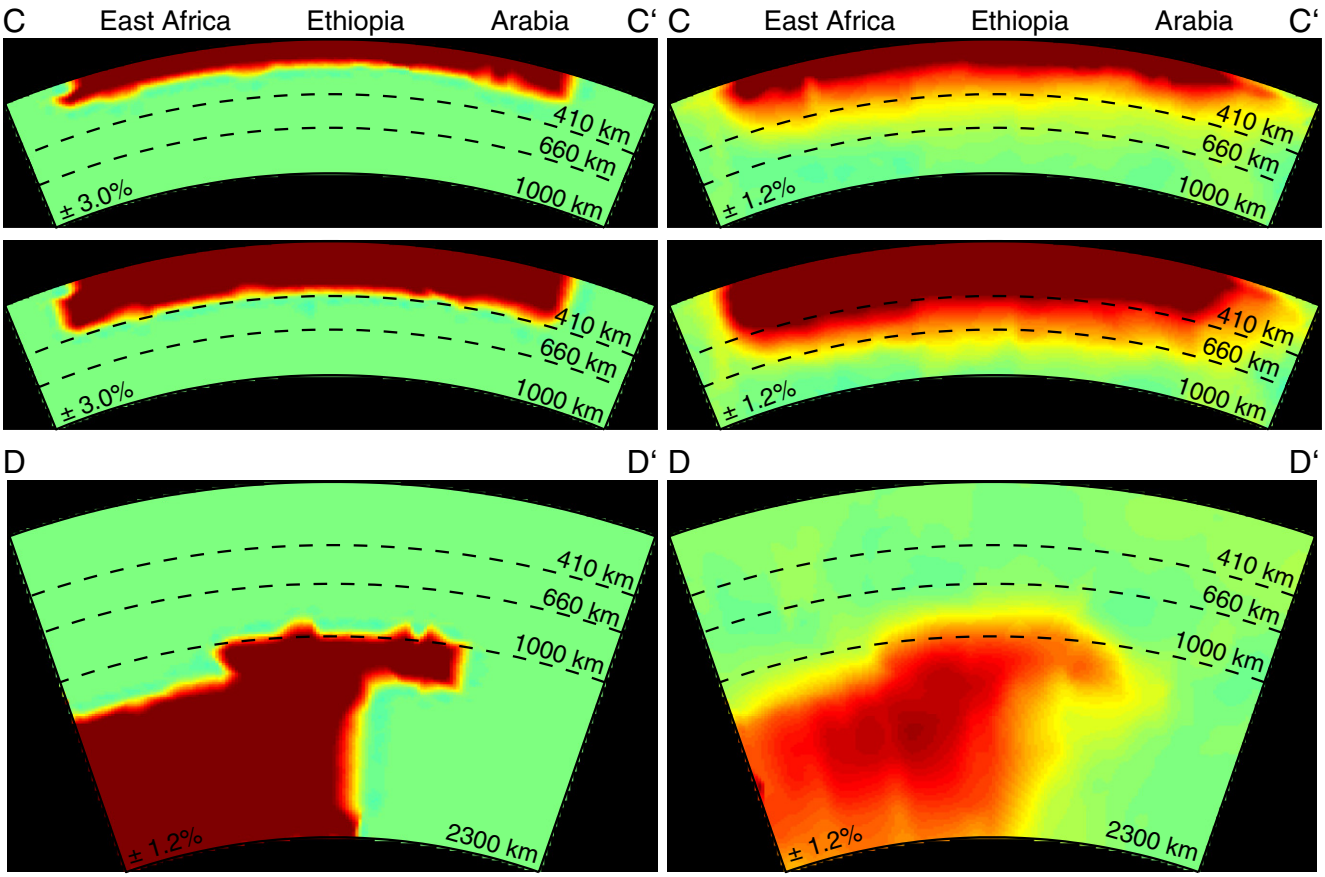

Fig. 6. Vertical resolution tests. Synthetic tests to examine the extent of vertical smearing in our model. Input models are shown on the left and recovered models are shown on the right, and the anomalies have been projected onto the adaptive grid (Supplemental Fig. 2). The top and middle examples show an upper mantle low-velocity anomaly extending to 200 and 400 km depth, respectively, beneath eastern Africa and Arabia. The bottom example shows a low-velocity anomaly with structure similar to the superplume beneath southern Africa. Refer to Figs. 3 and 8 for the locations of profiles C–C′ and D–D′, respectively.

for example, suggested that a single plume beneath southern Ethiopia could explain the distribution of magmatism and uplift throughout the AARS if the plume material spread laterally, guided by lithospheric topography. In contrast, Montelli et al. (2006) imaged low-velocity features beneath both Afar and East Africa, which they suggest are separate plumes that originate at mid-mantle depths or deeper. Other studies have also advocated for multiple plumes beneath the study region. Burke (1996) interpreted different episodes of volcanism as originating from different plumes, including one plume centered beneath southern Ethiopia, another beneath Afar, and a third beneath central Kenya. Camp and Roobol (1992) suggested that a plume might also exist beneath the Arabian Shield. Chang and Van der Lee (2011) imaged two plumes beneath Kenya and Afar, with a third plume beneath northern Arabia. The presence of multiple plumes has also been suggested from the analysis of gravity (Ebinger et al., 1989), geochronologic (George et al., 1998), and geochemical (George et al., 1998; Nelson et al., 2008; Pik et al., 2006) data and some models of mantle convection (Lin et al., 2005).

Assessing the number of plumes that may have impinged on the lithosphere beneath the AARS could be difficult to accomplish with seismic tomography because if multiple plumes are present, it is possible that their corresponding plume head material could have spread laterally, coalescing into one larger feature. This would appear as a continuous, low-velocity anomaly in the upper mantle, somewhat similar to that seen in our model. Plume tails are also notoriously difficult to image (*e.g.* Hwang et al., 2011; Montelli et al., 2006). However, the depth extent (~500–700 km; Fig. 4) of the low-velocity region we have imaged beneath the AARS provides important constraints in evaluating the plume model. The 200-km thick, upper mantle synthetic anomaly shown in the resolution tests in Fig. 6 provides a reasonable approximation to one or more plume heads that have spread laterally beneath the study area. As shown in the recovered image (Fig. 6), the low-velocity structure smears downwards by ~200 km, but this is not deep enough to be consistent with the depth extent of the low-velocity region in our model (Fig. 4).

For the plume model to create an upper mantle anomaly that would be consistent with our results, material from multiple plume heads would need to extend to depths of ~400–500 km beneath the AARS (Fig. 6). Laboratory and numerical models indicate that this may be possible if the starting plume heads were ascending through the transition zone (Davaille et al., 2005; Sleep, 1997; van Keken, 1997). However, rifting, volcanism, and plateau uplift have been occurring for tens of millions of years across much of eastern Africa and western Arabia, including the eruption of flood basalts in Ethiopia-Afar at ~30 Ma (Hofmann et al., 1997; Mohr, 1983). After this, plume material would have flattened against the lithosphere within the upper ~200 km of the mantle (Davaille et al., 2005; Sleep, 1997; van Keken, 1997). Therefore, even if multiple plume heads are invoked, the roughly uniform thickness (~500–700 km) of the low-velocity region imaged beneath eastern Africa and Arabia is not easily accounted for by the plume model.

5.2. Small-scale convection models

A second group of models that have been suggested to explain the origin of the AARS invoke small-scale convection. Some studies, such as King and Ritsema (2000) and King (2007), attribute the convection

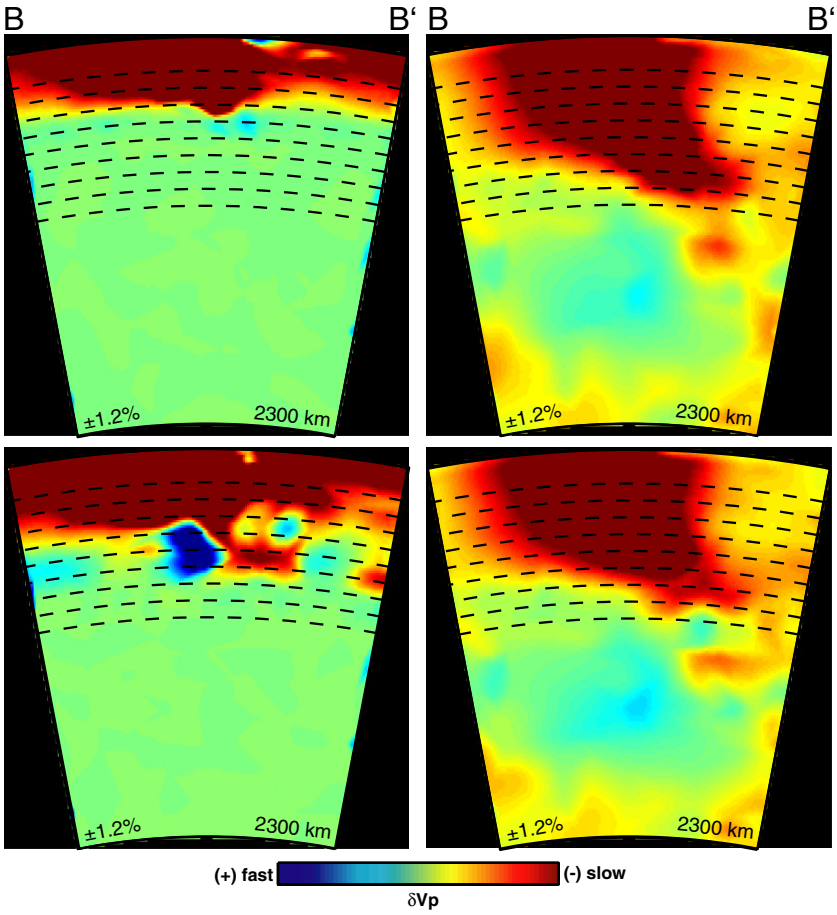

Fig. 7. Squeeze tests. Examples of squeeze tests, examining the mantle structure along profile B–B′ (Figs. 3–4). Dashed lines mark depths of 200–1000 km in 100 km increments. The models on the left have been squeezed to (top) 500 and (bottom) 800 km, respectively. The models on the right are the corresponding results of the full, two-stage squeezed inversion. Note that when the model is not "oversqueezed" (as in the 500 km case), the low-velocity structure does retreat to slightly shallower depths.

to edge-flow (Fig. 2b), where differences in heat flux between the thicker lithosphere beneath the Congo craton and thinner lithosphere beneath the surrounding mobile belts lead to rifting above a small-scale thermal upwelling. However, the effects of edge-flow convection are shallow, confined to depths less than ~350 km, and do not extend over as large an area as that shown in our P-wave tomographic image (King, 2007; King and Ritsema, 2000). Other studies have argued that extensional stresses along the edges of the African plate induce small-scale convection beneath the stretched lithosphere (Buck, 1986; Mutter et al., 1988; Fig. 2a). Given the small amount (<10%) of lithospheric extension in eastern Africa, it is unlikely that small-scale convective instabilities arising from lithospheric thinning would extend through the entire upper mantle (Buck, 1986; Mutter et al., 1988), as shown in our results. Therefore, our P-wave tomography model is also inconsistent with this type of geodynamic model.

5.3. Superplume model

The third type of model attributes the origin of the AARS and the associated perturbed upper mantle to the African superplume, a large, thermo-chemical anomaly that develops near the core-mantle boundary beneath southern Africa and tilts northeastward beneath eastern Africa at mid-mantle depths (Fig. 2d; Li et al., 2008; Montelli et al., 2006; Ritsema et al., 1998b, 1999, 2011; Simmons et al., 2007, 2009, 2010). As mentioned previously, numerous tomographic models (Bastow et al., 2005, 2008; Benoit et al., 2006b; Park and Nyblade, 2006; Park et al., 2007, 2008; Ritsema et al., 1999) have suggested that the anomalous upper mantle structure beneath the AARS represents a continuation of the lower-mantle superplume anomaly into the upper mantle. Some mantle convection models indicate that dynamic topography supported by the superplume can explain both the high surface elevations observed across southern and eastern Africa (Forte et al., 2010; Gurnis et al., 2000; Lithgow-Bertelloni and Silver, 1999; Moucha and Forte, 2011) as well as the tilt of the Arabian plate (Daradich et al., 2003). Major and trace element compositions of basalts across eastern Africa are also consistent with the superplume model (Furman, 2007; Furman et al., 2006).

To explore the potential connectivity between the AARS and the superplume, an additional set of resolution tests was performed using synthetic anomalies in both the upper and lower mantle (Fig. 8). To mimic the continuous low-velocity structure across mid-mantle depths seen in our model (Fig. 4), the synthetic results indicate that the superplume anomaly must extend upwards to depths of at least ~1100 km, shallower than the ~1500 km depth reported in other studies (*e.g.* Montelli et al., 2006; Ritsema et al., 1998b; Simmons et al., 2007, 2009, 2010). Given the vertical smearing of both the lower and upper mantle anomalies, these features could be separated by up to ~400 km, and so it is difficult to say with certainty if the anomalies are connected across the transition zone. However, given the close proximity of the anomalies, it is plausible that there could exist a geodynamic connection between them. As outlined in Sections 5.1–5.2, neither the plume nor small-scale convection models are consistent with the upper mantle low-velocity region imaged in our study. Given these observations, and

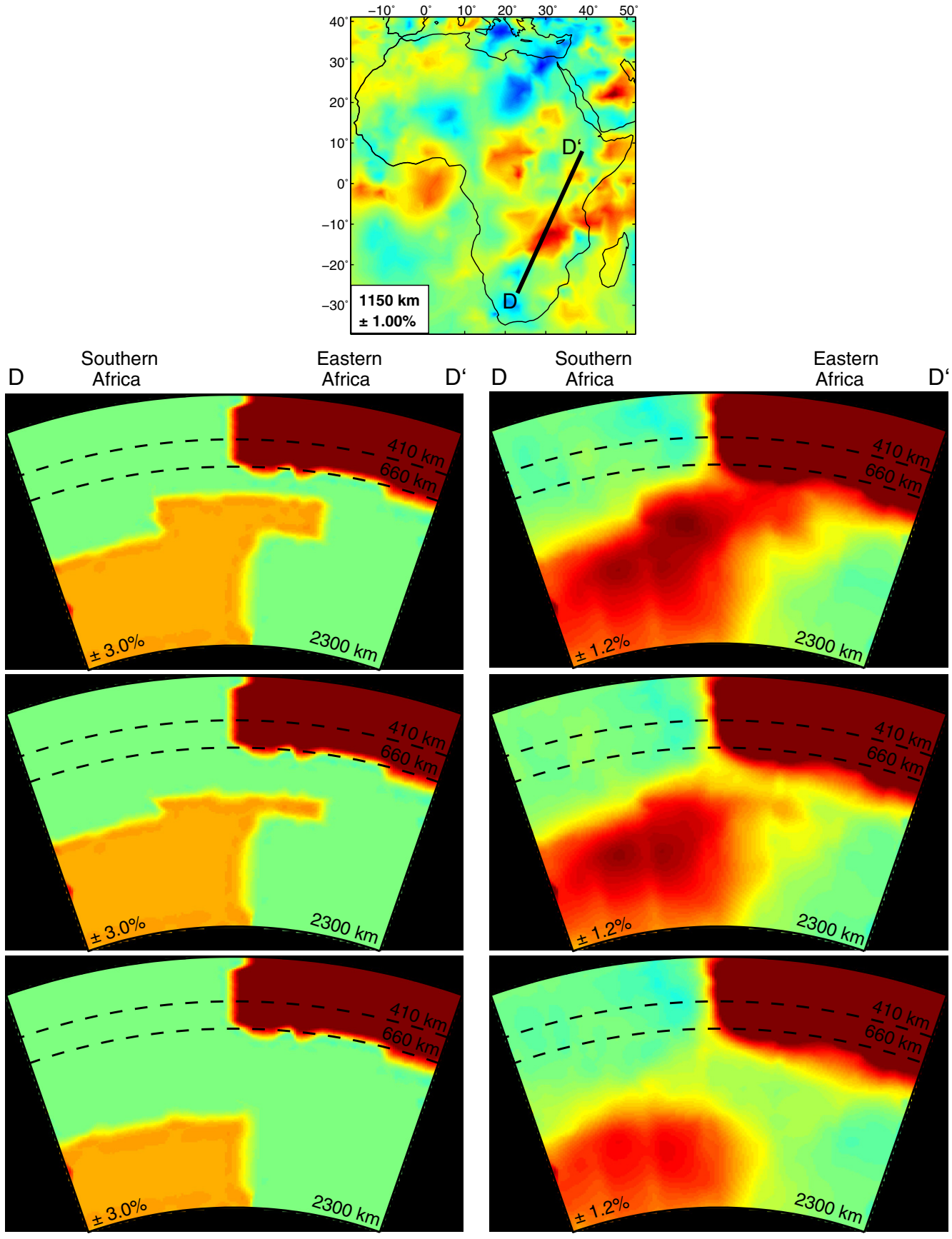

Fig. 8. Assessment of the superplume model. (top) Map showing the location of profile D–D′. (bottom) Cross-sections along profile D–D′, with input models on the left and recovered models on the right. The synthetic anomalies have been projected onto the adaptive grid (Supplemental Fig. 2). The upper and lower mantle structures were progressively separated to examine their potential connectivity. The top of the lower mantle anomaly is at 900 km, 1100 km, and 1500 km depth in the upper, middle, and lower panels, respectively. Similar to the vertical resolution tests (Fig. 6), the upper mantle anomaly has an input amplitude of 3% and the lower mantle anomaly has an input amplitude of 1.2%.

given that the superplume anomaly rises to fairly shallow (at least ~1100 km) depths in the mantle, we favor the superplume model to explain the pattern of P-wave velocity variations in our tomographic image and consequently the origin of the AARS.

It is interesting to note that the low-velocity anomaly beneath Ethiopia-Afar (Fig. 3) has a more pronounced signature than the rest of the AARS. Using global tomography and fluid mechanics constraints, Davaille et al. (2005) has suggested that Afar may be underlain by a plume whose connection to the lower mantle has disappeared. As discussed in Sections 5.1 and 5.3, the vertical extent of the upper mantle low-velocity anomaly in our model is not consistent with plume material that has flattened against the base of the lithosphere, and we instead favor the superplume model. However, we also suggest that a superplume–plume hybrid model might also be possible. If plume material such as that described by Davaille et al. (2005) has become entrained in the low-velocity material beneath the AARS that originated from the superplume, this could possibly explain why the observed velocity perturbations in this region are more pronounced and why the Afar region has a geochemical signature that may be different than that in East Africa (*e.g.* George et al., 1998; Nelson et al., 2008; Pik et al., 2006; Rogers et al., 2000). However, we would still argue that the superplume model is dominantly responsible for driving the Cenozoic tectonism in the AARS.

6. Summary

Using an adaptively parameterized tomography approach and travel-times from earthquakes recorded on many new permanent and temporary seismic stations, we have developed a new image of P-wave speed variations in the mantle which reveals a laterally continuous low-velocity anomaly beneath eastern Africa and western Arabia, extending to a depth of ~500–700 km. Our model also shows a continuous low-velocity structure at mid-mantle depths connecting the lower mantle African superplume structure to the anomalous upper mantle beneath eastern Africa. Resolution tests indicate that there is ~200 km of vertical smearing in our model, and thus the top of the African superplume is likely at a depth of ~1100 km or less.

We have used these observations to evaluated geodynamic models for the origin of Cenozoic tectonism in the AARS. Models which invoke one or more plume heads are difficult to reconcile with the lateral and depth extent of the upper mantle low-velocity anomaly, as are non-plume models invoking small-scale convection passively induced by lithospheric extension or by edge-flow around thick cratonic lithosphere. Instead, the upper mantle anomaly beneath eastern Africa and western Arabia can be explained by the superplume model, where the anomalous upper mantle structure is a continuation of a large, thermo-chemical upwelling in the lower mantle beneath southern Africa. This finding provides further support for a geodynamic connection between processes in the Earth's lower mantle and continental break-up within the AARS, as has been argued for previously by many authors.

Acknowledgments

We thank A. Reusch, I. Bastow, G. Mulibo, and Y. Park for providing the P-wave travel-time data from their respective studies, R. van der Hilst and S. Burdick for providing the tomography software, and R. van der Hilst as well as two anonymous reviewers for helpful comments that improved this paper. The Incorporated Research Institutions for Seismology (IRIS) Data Management System provided data handling assistance, and funding for this project was provided by the National Science Foundation (grant numbers OISE 0530062, EAR 0824781, and EAR 0440032).

Appendix A. Supplementary data

Supplementary data to this article can be found online at doi:10.1016/j.epsl.2011.12.023.

References

Abers, G.A., Roecker, S.W., 1991. Deep-structure of an arc-continent collision: earthquake relocation and inversion for upper mantle P and S wave velocities beneath Papua New Guinea. J. Geophys. Res. 96, 6379–6401.
Allen, R.M., Tromp, J., 2005. Resolution of regional seismic models: squeezing the Iceland anomaly. Geophys. J. Int. 161, 373–386.
Bassin, C., Laske, G., Masters, G., 2000. The current limits of resolution for surface wave tomography in North America. EOS Trans. AGU 81 (48) Fall Meet. Suppl., Abstract S12A-03.
Bastow, I.D., Stuart, G.W., Kendall, J.-M., Ebinger, C.J., 2005. Upper-mantle seismic structure in a region of incipient continental breakup: northern Ethiopian rift. Geophys. J. Int. 162, 479–493.
Bastow, I.D., Nyblade, A.A., Stuart, G.W., Rooney, T.O., Benoit, M.H., 2008. Upper mantle seismic structure beneath the Ethiopian hot spot: rifting at the edge of the African low-velocity anomaly. Geochem. Geophys. Geosyst. 9. doi:10.1029/2008GC002107.
Benoit, M.H., Nyblade, A.A., VanDecar, J.C., Gurrola, H., 2003. Upper mantle P wave velocity structure and transition zone thickness beneath the Arabian Shield. Geophys. Res. Lett. 30. doi:10.1029/2002GL016436.
Benoit, M.H., Nyblade, A.A., Owens, T.J., Stuart, G., 2006a. Mantle transition zone structure and upper mantle S velocity variations beneath Ethiopia: evidence for a broad, deep-seated thermal anomaly. Geochem. Geophys. Geosyst. 7. doi:10.1029/2006GC001398.
Benoit, M.H., Nyblade, A.A., VanDecar, J.C., 2006b. Upper mantle P-wave speed variations beneath Ethiopia and the origin of the Afar hotspot. Geology 34, 329–332.
Bijwaard, H., Spakman, W., Engdahl, E.R., 1998. Closing the gap between regional and global travel time tomography. J. Geophys. Res. 103, 30055–30078.
Buck, W.R., 1986. Small-scale convection induced by passive rifting: the cause for uplift of rift shoulders. Earth Planet. Sci. Lett. 77, 362–372.
Burke, K., 1996. The African plate. S. Afr. J. Geol. 99, 341–409.
Camp, V.E., Roobol, M.J., 1992. Upwelling asthenosphere beneath western Arabia and its regional implications. J. Geophys. Res. 97, 15255–15271.
Chang, S.-J., Van der Lee, S., 2011. Mantle plumes and associated flow beneath Arabia and East Africa. Earth Planet. Sci. Lett.. doi:10.1016/j.epsl.2010.12.050.
Chang, S.-J., Merino, M., Van der Lee, S., Stein, S., Stein, C.A., 2011. Mantle flow beneath Arabia offset from the opening Red Sea. Geophys. Res. Lett. 38. doi:10.1029/2010GL045852.
Daradich, A., Mitrovica, J.X., Pysklywec, R.N., Willett, S.D., Forte, A.M., 2003. Mantle flow, dynamic topography, and rift-flank uplift of Arabia. Geology 31, 901–904.
Davaille, A., Stutzmann, E., Silveira, G., Besse, J., Courtillot, V., 2005. Convective patterns under the Indo-Atlantic "box". Earth Planet. Sci. Lett. 239, 233–252.
Debayle, E., Lévêque, J., Cara, M., 2001. Seismic evidence for a deeply rooted low-velocity anomaly in the upper mantle beneath the northeastern Afro/Arabian continent. Earth Planet. Sci. Lett. 193, 423–436.
Ebinger, C.J., Sleep, N.H., 1998. Cenozoic magmatism throughout east Africa resulting from impact of a single plume. Nature 395, 788–791.
Ebinger, C., Bechtel, T., Forsyth, D., Bowin, C., 1989. Effective elastic plate thickness beneath the East African and the Afar plateau and dynamic compensation for the uplifts. J. Geophys. Res. 94, 2883–2901.
Engdahl, E.R., van der Hilst, R.D., Buland, R., 1998. Global teleseismic earthquake relocation with improved travel times and procedures for depth determination. Bull. Seismol. Soc. Am. 88, 722–743.
Fishwick, S., 2010. Surface wave tomography: imaging of the lithosphere-asthenosphere boundary beneath central and southern Africa? Lithos 120, 63–73.
Forte, A.M., Quéré, S., Moucha, R., Simmons, N.A., Grand, S.P., Mitrovica, J.X., Rowley, D.B., 2010. Joint seismic-geodynamic-mineral physical modeling of African geodynamics: a reconciliation of deep-mantle convection with surface geophysical constraints. Earth Planet. Sci. Lett. 295, 329–341.
Fouch, M.J., James, D.E., VanDecar, J.C., van der Lee, S., Group Kaapvaal Seismic, 2004. Mantle seismic structure beneath the Kaapvaal and Zimbabwe Cratons. S. Afr. J. Geol. 107, 33–44.
Furman, T., 2007. Geochemistry of East African Rift basalts: an overview. J. Afr. Earth Sci. 48, 147–160.
Furman, T., Bryce, J., Rooney, T., Hanan, B., Yirgu, G., Ayalew, D., 2006. Heads and tails: 30 million years of the Afar plume, in The Afar Volcanic Province within the East African Rift System. Geol. Soc. Spec. Publ. 259, 95–119.
George, R., Rogers, N., Kelley, S., 1998. Earliest magmatism in Ethiopia: evidence for two mantle plumes in one flood basalt province. Geology 26, 923–926.
Grand, S., 2002. Mantle shear-wave tomography and the fate of subducted slabs. Phil. Trans. Roy. Soc. London A360, 2475–2491.
Gu, Y.J., Dziewonski, A.M., Su, W., Ekstrom, G., 2001. Models of the mantle shear velocity and discontinuities in the pattern of lateral heterogeneity. J. Geophys. Res. 106, 11169–11199.
Gurnis, M., Mitrovica, J.X., Ritsema, J., van Heijst, H.J., 2000. Constraining mantle density structure using geological evidence of surface uplift rates: the case of the African superplume. Geochem. Geophys. Geosyst. 3. doi:10.1029/1999GC000035.
Hofmann, C., Courtillot, V., Feraud, G., Rochette, P., Yirgu, G., Ketefo, E., Pik, R., 1997. Timing of the Ethiopian flood basalt event and implications for plume birth and global change. Nature 389, 838–841.

Hwang, Y.K., Ritsema, J., van Keken, P.E., Goes, S., Styles, E., 2011. Wavefront healing renders deep plumes seismically invisible. Geophys. J. Int. 187, 273–277.
Kárason, H., 2002. Constraints on Mantle Convection from Seismic Tomography and Flow Modeling. Ph.D. thesis, Massachusetts Institute of Technology.
Kárason, H., van der Hilst, R.D., 2000. Constraints on mantle convection from seismic tomography. in history and dynamics of plate motion. In: Richards, M.A., Gordon, R., van der Hilst, R.D. (Eds.), Geophys. Monogr. Ser., 121. AGU, Washington, D.C, pp. 277–288.
Kárason, H., van der Hilst, R.D., 2001. Tomographic imaging of the lowermost mantle with differential times of refracted and diffracted core phases (PKP, Pdiff). J. Geophys. Res. 106, 6569–6587.
Kennett, B.L.N., Engdahl, E.R., Buland, R., 1995. Constraints on seismic velocities in the Earth from travel times. Geophys. J. Int. 122, 108–124.
King, S.D., 2007. Hotspots and edge-driven convection. Geology 35, 223–226.
King, S.D., Ritsema, J., 2000. African hot spot volcanism: small-scale convection in the upper mantle beneath cratons. Science 290, 1137–1140.
Li, C., van der Hilst, R.D., Toksöz, M.N., 2006. Constraining P wave velocity variations in the upper mantle beneath Southeast Asia. Phys. Earth Planet. Inter. 154, 180–195.
Li, C., van der Hilst, R.D., Engdahl, E.R., Burdick, S., 2008. A new global model for 3-D variations of P-wave velocity in the Earth's mantle. Geochem. Geophys. Geosyst. 9. doi:10.1029/2007GC001806.
Lin, S.-C., Kuo, B.-Y., Chiao, L.-Y., van Keken, P.E., 2005. Thermal plume models and melt generation in East Africa: a dynamic modeling approach. Earth Planet. Sci. Lett. 237, 175–192.
Lithgow-Bertelloni, C., Silver, P.G., 1999. Dynamic topography, plate driving forces and the African Superswell. Nature 395, 269–272.
Masters, T.G., Laske, G., Bolton, H., Dziewonski, A., 2000. The relative behavior of shear velocity, bulk sound speed, and compressional velocity in the mantle: implications for chemical thermal structure, in Earth's deep interior: mineral physics and tomography from the atomic to the global scale. Geophys. Mono. 117, 63–87.
Mégnin, C., Romanowicz, B., 2000. The three-dimensional shear velocity structure of the mantle from the inversion of body, surface, and higher-mode waveforms. Geophys. J. Int. 143, 709–728.
Mohr, P., 1983. Ethiopian flood basalt province. Nature 303, 577–584.
Montelli, R., Nolet, G., Dahlen, F.A., Masters, G., 2006. A catalogue of deep mantle plumes: New results from finite-frequency tomography. Geochem. Geophys. Geosyst. 7. doi:10.1029/2006GC001248.
Moucha, R., Forte, A.M., 2011. Changes in African topography drive by mantle convection. Nat. Geosci. 4, 707–712.
Mulibo, G., Nyblade, A., Tugume, F., 2011. Mantle structure beneath East Africa and Zambia from body wave tomography. EOS Trans. AGU Fall Meet. Suppl., Abstract, T32A-03..
Mutter, J.C., Buck, W.R., Zehnder, C.M., 1988. Convective partial melting: a model for the formation of thick basaltic sequences during the initiation of spreading. J. Geophys. Res. 93, 1031–1048.
Nelson, W.R., Furman, T., Hanan, B., 2008. Sr, Nd, Pb, and Hf evidence for two-plume mixing beneath the East African Rift system. Geochim. Cosmochim. Acta 72, A676.
Nolet, G., 1985. Solving or resolving inadequate and noisy tomographic systems. J. Comput. Phys. 61, 463–482.
Nyblade, A.A., Owens, T.J., Gurrola, H., Ritsema, J., Langston, C.A., 2000. Seismic evidence for a deep upper mantle thermal anomaly beneath east Africa. Geology 28, 599–602.
Paige, C.C., Saunders, M.A., 1982. LSQR: an algorithm for sparse linear equations and sparse least squares. ACM Trans. Math. Software 8, 43–71.
Park, Y., Nyblade, A., 2006. P-wave tomography reveals a westward dipping low velocity zone beneath the Kenya Rift. Geophys. Res. Lett. 33, 1–4.
Park, Y., Nyblade, A.A., Rodgers, A.J., Al-Amri, A., 2007. Upper mantle structure beneath the Arabian Peninsula and northern Red Sea from teleseismic body wave tomography: implications for the origin of Cenozoic uplift and volcanism in the Arabian Shield. Geochem. Geophys. Geosyst. 8. doi:10.1029/2006GC001566.
Park, Y., Nyblade, A.A., Rodgers, A.J., Al-Amri, A., 2008. S wave velocity structure of the Arabian Shield upper mantle from Rayleigh wave tomography. Geochem. Geophys. Geosyst. 9. doi:10.1029/2007GC001895.
Pasyanos, M.E., Nyblade, A.A., 2007. A top to bottom lithospheric study of Africa and Arabia. Tectonophysics 444, 27–44.
Pik, R., Marty, B., Hilton, D.R., 2006. How many mantle plumes in Africa? The geochemical point of view. Chem. Geol. 226, 100–114.
Priestley, K., McKenzie, D., Debayle, E., Pilidou, S., 2008. The African upper mantle and its relationship to tectonics and surface geology. Geophys. J. Int. 175, 1108–1126.
Reusch, A.M., 2009. Using Seismic Data to Interpret the Mechanism for Cenozoic Volcanism beneath Ross Island, Antarctica, and the Cameroon Volcanic Line, West Africa. Ph.D. thesis, The Pennsylvania State University.
Ritsema, J., Nyblade, A.A., Owens, T., Langston, C., VanDecar, J., 1998a. Upper mantle seismic velocity structure beneath Tanzania, East Africa: implications for the stability of cratonic lithosphere. J. Geophys. Res. 103, 21201–21213.
Ritsema, J., Ni, S., Helmberger, D.V., Crotwell, H.P., 1998b. Evidence for strong shear velocity reductions and velocity gradients in the lower mantle beneath Africa. Geophys. Res. Lett. 25, 4245–4248.
Ritsema, J., van Heijst, H.J., Woodhouse, J.H., 1999. Complex shear wave velocity structure beneath Africa and Iceland. Science 286, 1925–1928.
Ritsema, J., Deuss, A., van Heijst, H.J., Woodhouse, J.H., 2011. S40RTS: a degree-40 shear-velocity model for the mantle from new Rayleigh wave dispersion, teleseismic traveltime and normal-mode splitting function measurements. Geophys. J. Int. 184, 1223–1236.
Rogers, N., Macdonald, R., Fitton, J.G., George, R., Smith, M., Barreiro, B., 2000. Two mantle plumes beneath the East African rift system: Sr, Nd, and Pb isotope evidence from Kenya Rift basalts. Earth Planet. Sci. Lett. 176, 387–400.
Romanowicz, B., 2009. The thickness of tectonic plates. Science 324, 474–476.
Saltzer, R.L., Humphreys, E.D., 1997. Upper mantle P wave velocity structure of the eastern Snake River Plain and its relationship to geodynamic models of the region. J. Geophys. Res. 102, 11829–11841.
Schutt, D.L., Humphreys, E.D., 2004. P and S wave velocity and Vp/Vs in the wake of the Yellowstone hot spot. J. Geophys. Res. 109. doi:10.1029/2003JB002442.
Sebai, A., Stutzmann, E., Montagner, J.-P., Sicilia, D., Beucler, E., 2006. Anisotropic structure of the African upper mantle from Rayleigh and Love wave tomography. Phys. Earth Planet. Inter. 155, 48–62.
Sicilia, D., Montagner, J.-P., Cara, M., Stutzmann, E., Debayle, E., Lépine, J.-C., Lévêque, J.-J., Beucler, E., Sebai, A., Roult, G., Ayele, A., Sholan, J.M., 2008. Upper mantle structure of shear-waves velocities and stratification of anisotropy in the Afar Hotspot region. Tectonophysics 462, 164–177.
Simmons, N.A., Forte, A.M., Grand, S.P., 2007. Thermochemical structure and dynamics of the African superplume. Geophys. Res. Lett. 34. doi:10.1029/2006GL028009.
Simmons, N.A., Forte, A.M., Grand, S.P., 2009. Joint seismic, geodynamic and mineral physical constraints on three-dimensional mantle heterogeneity: implications for the relative importance of thermal versus compositional heterogeneity. Geophys. J. Int. 177, 1284–1304.
Simmons, N.A., Forte, A.M., Boschi, L., Grand, S.P., 2010. GyPSuM: a joint tomographic model of mantle density and seismic wave speeds. J. Geophys. Res. 115. doi:10.1029/2010JB007631.
Simmons, N.A., Myers, S.C., Johannesson, G., 2011. Global-scale P wave tomography optimized for prediction of teleseismic and regional travel times for Middle East events: 2. Tomographic inversion. J. Geophys. Res. 116. doi:10.1029/2010JB007969.
Sleep, N., 1997. Lateral flow and ponding of starting plume material. J. Geophys. Res. 102, 10001–10012.
Spakman, W., Nolet, G., 1988. Imaging algorithms, accuracy and resolution in delay time tomography. In: Vlaar, N.J. (Ed.), Mathematical Geophysics: A Survey of Recent Developments in Seismology and Geodynamics, pp. 155–188.
van Keken, P., 1997. Evolution of starting mantle plumes: a comparison between numerical and laboratory models. Earth Planet. Sci. Lett. 148, 1–11.
VanDecar, J., Crosson, R., 1990. Determination of teleseismic relative phase arrival times using multi-channel cross-correlation and least squares. Bull. Seismol. Soc. Am. 80, 150–169.
Weeraratne, D., Forsyth, D., Fischer, K., Nyblade, A., 2003. Evidence for an upper mantle mantle plume beneath the Tanzanian craton from Rayleigh wave tomography. J. Geophys. Res. 108, 1–7.
Wessel, P., Smith, W., 1998. New, improved version of the generic mapping tools released. EOS Trans. AGU 79, 579.